JOURNAL OF
EMERGING INVESTIGATORS

Article

Influence of induction heating on static recrystallization kinetics of AISI 4130 steel

Eric J. Chen[1], Yonguk Lee[2], Megan E. Hurley[2], Victoria M. Miller[2]

[1] Seminole High School, Sanford, Flordia

[2] Department of Materials Science and Engineering, University of Florida, Gainesville, Florida

SUMMARY

Most metals used in industrial applications undergo at least one form of heat treatment to enhance their mechanical properties. Induction heating is an attractive energy-efficient alternative to conventional radiant heating methods, but its widespread industrial adoption is hindered by fundamental knowledge gaps. To remedy this, this study aims to investigate the effects induction heating has on static recrystallization kinetics and microstructural evolution of American Iron and Steel Institute 4130 steel. We hypothesize that induction heating, like other electric current-based techniques, will accelerate the recrystallization rate of the investigated 4130 steel samples. Microhardness measurements and optical and scanning electron microscopy images were collected after heating the 4130 steel samples for varying times using an induction heater. These results were then compared to those obtained from traditional radiant heat treatments performed with identical heating profiles in a muffle furnace. Overall, our results indicate accelerated static recrystallization kinetics and microstructural evolution among the induction-heated samples. However, results also suggest that induction heating impacts other metallurgical phenomena such as pearlite spheroidization and electron-crystal interactions. Further investigation is needed to decouple these additional effects and optimize heating pathways, paving the way for induction heating technologies to become a leading method in metal heat treatments.

INTRODUCTION

In industry, it is rare for a metal to go through the manufacturing process without being heat-treated at least once. In fact, the global heat treatment market was estimated at around $110 billion in 2024, reflecting its indispensable role in automotive, aerospace, and energy sectors (1). Heat treatments alter a material's properties through controlled heating and cooling, enabling engineers to optimize characteristics like hardness, strength, and toughness. For instance, rapid cooling can increase the hardness and strength of a medium-carbon steel, with compensated ductility loss (2). As the mechanical and physical properties of all materials depend heavily on their microstructure, developing more efficient heat-treatment technologies to replace traditional energy inefficient methods requires a thorough analysis of microstructural evolution.

In the context of heat treatments, prolonged exposure to high temperatures, especially when influenced by deformation, often alters the microstructure of metals, specifically by causing recovery and recrystallization (RX) phenomena to occur (2). Researchers commonly study RX in two ways: statically and dynamically. Static recrystallization (SRX) occurs when a material is deformed before the recrystallization process and heating, while dynamic recrystallization (DRX) takes place when the material is hot-deformed during the recrystallization heat treatment (2). On the microscopic scale, deforming a material increases the density of dislocations–linear defects in the crystal structure where atoms are out of alignment (2, 3). This increase in dislocations causes the hardening of metals and strains grains, which are regions where atoms are arranged in a continuous, orderly pattern (2, 3). During heat treatment, recovery and RX reduce the dislocation density by replacing the strained grains with new, strain-free grains (3). These new grains make it easier to perform subsequent forming processes and, ultimately, achieve desired material properties (3).

Heat treatments can be performed in various ways, with notable heating techniques including radiative furnaces, Joule effect heating, and induction heating (4-6). Joule effect heating involves inducing a direct electrical pulse through a conductive sample via direct contact with a current-carrying wire (4). This can be achieved either by imposing short electrical pulses lasting a few microseconds to limit temperature increase, or by applying direct Joule effect heating for prolonged periods (7-10). Similarly, induction heating also involves inducing an electrical current, but its method is different. Using a solenoid coil carrying a current, induction heating creates a magnetic field around the sample, which induces electric currents within the material (6). Of particular industrial interest, induction heating and other current-based methods are less energy-intensive and more cost-efficient for heat treating steels and other conductive metals compared to traditional radiative heating technologies (11). However, as a relatively novel heat treatment technique, induction heating has not been as extensively investigated as other electric current-based methods.

While some previous studies suggest that electric current flow has no significant consequences on the microstructural evolution of metals, more recent research has observed otherwise (4, 7-10, 12, 13). It is known that in metals, flowing electrons can delay dislocation motion and induce dislocation drag (13). In theory, this should produce a lower RX rate, but this contradicts previous literature. Alternatively, it has been suggested that drift electrons may promote and increase dislocation motion in metals by providing an additional driving force (4, 14-16). This phenomenon, known as the electron wind effect, is commonly attributed to an increased recrystallization

https://doi.org/10.59720/24-273

rate. Additionally, it was observed that the degree to which the electron wind effect accelerated RX in cold-worked copper depended on the amount of strain induced in the sample (17). However, the true implications of electric current flow induced during heat treatments, particularly by induction heating, remain not fully explored.

Previous studies have observed accelerated SRX kinetics in several metals, such as pure copper, a titanium alloy, an austenitic stainless steel, and an aluminum alloy, when heat-treated via an electric current, regardless of the applied current density (7-10). Similarly, exposure to an electrical current flow has consistently increased the rate of DRX, although this type of RX has been less thoroughly studied compared to SRX (4, 5, 18). While recent efforts have aimed to more thoroughly investigate the effects of electric current heat treatments on SRX and DRX in different metal alloy systems, the majority of studies have focused on Joule effect heating rather than induction heating. Additionally, only a few studies have explored microstructural evolution under induction heating, specifically using a magnesium-manganese alloy, a titanium alloy, and a nickel-based superalloy. However, SRX was not the focal point of these investigations, leaving a significant gap in understanding the correlation between these principles (16-18).

Furthermore, additional microstructural changes and phenomena can occur due to temperature gradients within a metal sample, caused by the uneven distribution of electrical currents generated by induction heating (10, 19, 20). The extent of this temperature gradient is material specific and is known as the skin effect. This effect arises from the tendency of alternating currents to flow along the surface of a conductive material rather than evenly through its cross-section (20). While the skin effect is a well-known and often anticipated consequence of induction heating, its impact on SRX has received minimal investigation (20). This is particularly concerning, as we anticipate that the skin effect will lead to faster RX rates and significant changes in microstructural evolution.

The present study focuses on American Iron and Steel Institute (AISI) 4130 steel, a low-alloy, medium-carbon steel commonly used in the automotive and aeronautical industries for steering, engines, suspensions, and transmissions (21). During manufacturing, these parts undergo complex forging routes that involve multiple cold/hot deformations, heat treatments, and quenches, during which the microstructure of the steel is heavily influenced by the process of RX (2, 4, 7). Therefore, understanding the RX kinetics involved in these forging routes and the resulting mechanical properties is of utmost importance.

We hypothesized that induction heating, similar to other current-based heat treatments, would accelerate SRX kinetics due to induced drift electrons, compared to traditional radiant heat treatments. To investigate this, we received AISI 4130 steel samples and subjected them to an initial homogenization heat treatment to remove any residual strain energy accumulated during previous processing. The homogenized samples were equally sectioned, compressed to induce deformation strains, and then heat-treated for varied time intervals under both traditional radiant and induction heating to induce RX. By performing Vickers microhardness measurements on the polished surfaces of the 4130 steel samples, we assessed the degree of strain energy present, indicating the extent of RX, completed at each time interval. This allowed us to compare the SRX kinetics of AISI 4130 steel heat-treated using induction heating to those from equivalent radiant heat treatments. The comparison aimed to evaluate the efficacy of induction heating technologies and assess the feasibility of implementing this relatively novel technology on an industrial scale.

Ultimately, our results show that induction heating dramatically accelerates the onset and completion of RX compared to traditional radiant heating, with microstructural

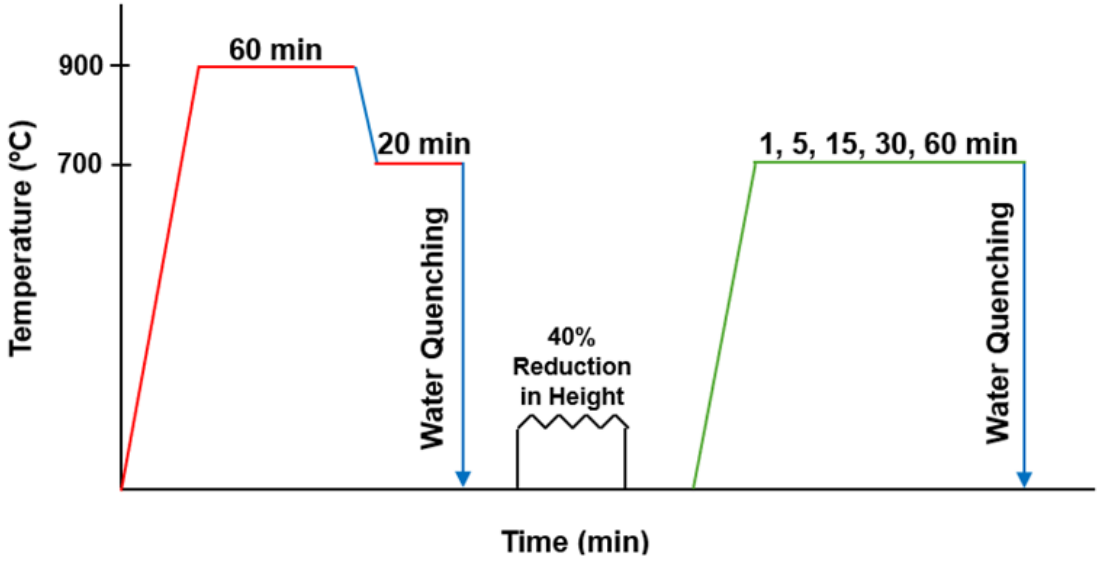

Figure 1: Heat treatment conditions used for static recrystallization of AISI 4130 steel. Samples first underwent a homogenization heat treatment (red) using radiant heating at 900°C for 60 minutes, then at 650°C for 20 minutes before water quenching to eliminate any residual strain. The samples were then deformed via compression to 40% of their original height. Finally, recrystallization heat treatments (green) were conducted using both radiant and induction heating at 700°C for hold times of 1, 5, 15, 30, and 60 minutes, followed by water quenching.

https://doi.org/10.59720/24-273

transformations such as grain nucleation occurring earlier and more rapidly. These observations support the hypothesis and suggest that induction heating may offer a viable, energy-efficient alternative for current steel heat treatments used in industry. However, certain observed microstructural phenomena, such as pearlite spheroidization, which occur in pearlite microstructures in steels but only after exceedingly long hold times, open up new questions that require further study to determine their cause and origins (2).

RESULTS

To validate our hypothesis that induction heating accelerates SRX kinetics more than radiant heating, we conducted equivalent heat treatments on AISI 4130 steel samples under both heating methods (**Figure 1**). We performed an initial homogenization heat treatment to eliminate residual strain from cold-forming and create near-identical ferrite/pearlite microstructures for comparison. We then sectioned and compressed samples to 40% of their original height to introduce the deformation strain necessary for RX (12). Finally, deformed samples underwent heat treatments at 700 °C in either a radiant or induction heating system for hold times ranging from one minute to one hour to induce SRX.

We examined samples from the same line of material preparations using an optical microscope (OM) and a scanning electron microscope (SEM) and collected Vickers microhardness measurements (HV) to study how the microstructure of AISI 4130 steel evolves during SRX. The latter technique involves pressing a precision diamond pyramid tip into the polished surface of a material and based on the applied load and the size of the resulting indent, the hardness value is calculated. Collected hardness measurements show that the AISI 4130 steel samples are significantly softer after induction heating than after radiant heating across all hold times (**Figure 2**). Even after just a 5-minute hold, the induction-heated samples have a statistically lower mean Vickers hardness of 200 ± 6 HV while the radiant-heated samples have one of 310 ± 5 HV, suggesting accelerated RX kinetics with induction heating.

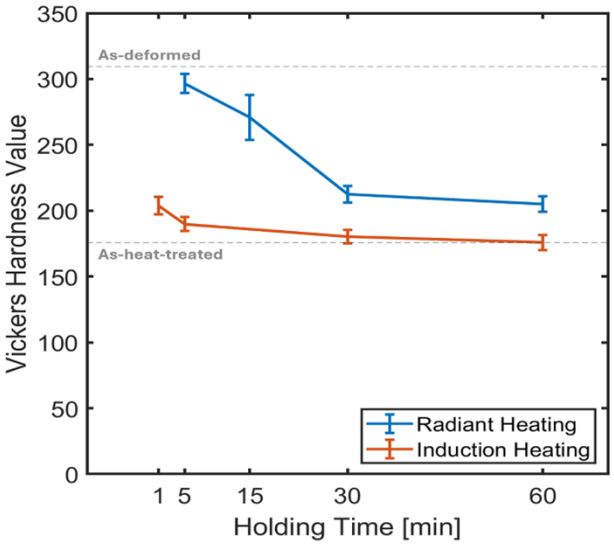

Figure 2: Vickers microhardness measurements as a function of holding time for both heating methods. From each sample, Vickers hardness measurements were collected near the center of the sample surface at five different points using an applied load of 0.3 kg. The "as-heat-treated" threshold corresponds to the mean sample hardness after the homogenization heat treatment, while the "as-deformed" threshold is based on the mean hardness of samples after deformation. Error bars represent the standard deviation, and two-tailed t-tests were used to determine statistical significance between both heating methods (p = 0.0002).

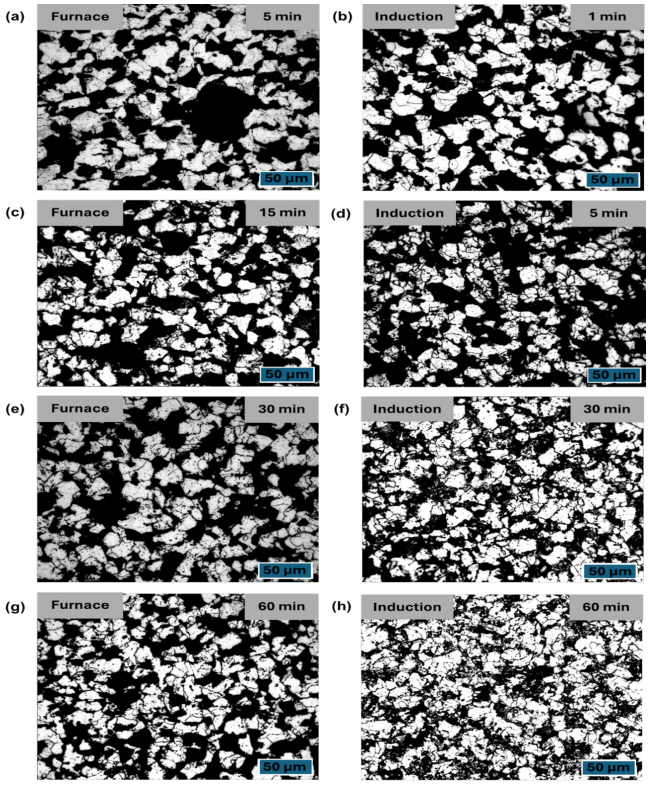

Figure 3: Comparing ferrite/pearlite microstructures of radiant- and induction-heated samples at varied holding times. A representative selection of optical microscopy (OM) images is shown for samples (A, C, E, G) radiantly and (B, D, F, H) inductively heated for (A) 5, (B) 1, (C) 15, (D) 5, (E, F) 30, and (G, H) 60 minutes, respectively. Light gray regions are ferrite, while darker regions are pearlite. The red boxes in (F) and (H) highlight regions with early signs of pearlite spheroidization, which is not observed in their radiantly heated counterparts.

While both heating methods generally show that the SRX phenomenon is induced in AISI 4130 steel, the induction-heated samples show an earlier onset of recrystallization and more pronounced grain nucleation (**Figure 3**). Recrystallized grains are typically more uniform, equiaxed, and smaller as they begin nucleating out from the older grains, making their presence visually distinct. In this instance, new RX grains appear as the breaking apart of light gray and dark gray areas in the collected OM images. Specifically, the light-gray areas are ferrite (a soft, low carbon phase) while the darker areas are pearlite, which consists of very thin alternating layers of ferrite and cementite (a hard, high carbon phase) that can be difficult to distinguish at low magnifications. This earlier onset of RX is distinctly apparent when comparing shorter hold

https://doi.org/10.59720/24-273

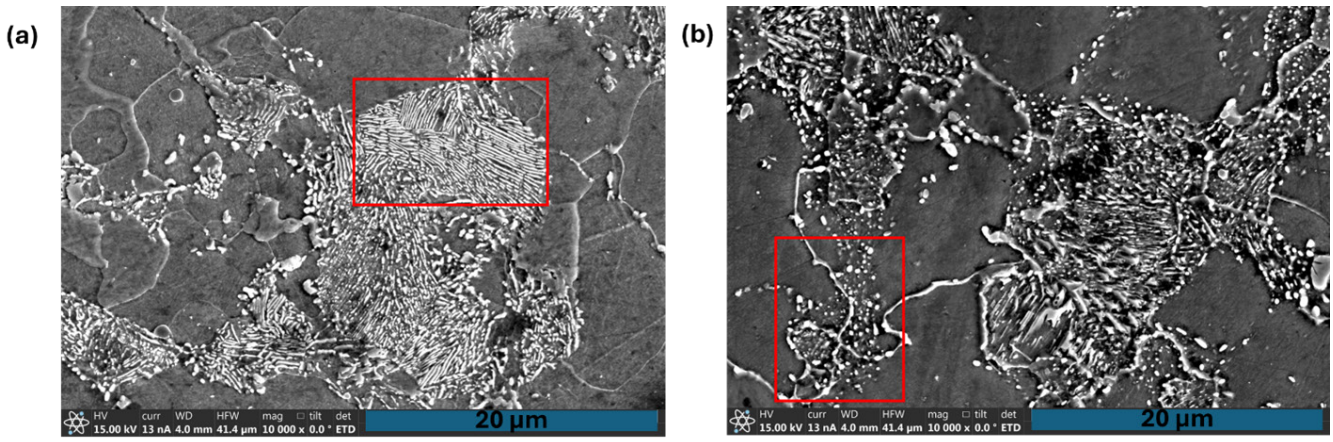

Figure 4: Induction heating encourages the spheroidization of pearlite microstructures. Scanning electron microscopy (SEM) images were collected from induction-heated samples with hold times of (A) one minute and (B) 30 minutes. As emphasized by the red boxes, the pearlite microstructure of the one minute heat treatment is perfectly intact with characteristic cementite lamellae (white, thin stacked layered regions), whereas after 30 minutes, the lamellae start to break down and spheroidize along grain boundaries.

times. Samples held for five minutes in radiant heating had only minor signs of SRX (**Figure 3A**). Conversely, samples held for just one minute in the induction heater showed clear signs of SRX, suggesting that the incubation time needed to initiate RX is far shorter for induction-heated samples (**Figure 3B**). Overall, recrystallized grains can be seen gradually invading and taking over the initially deformed grains. However, this progression occurs much more rapidly in the induction-heated samples, which contain a greater amount of new, nucleating ferrite grains compared to the radiantly-heated samples (**Figures 3C-H**).

Unexpectedly, the pearlite microstructures in the induction-heated samples appear to be undergoing spheroidization, specifically for the 30- and 60-minute hold times, whereas the radiantly heated samples do not (**Figures 3F-H**). This microstructural phenomenon can be seen more clearly by comparing SEM images taken after one and 30 minutes under induction heating (**Figure 4**). After one minute, the pearlite microstructure remains perfectly intact with distinct separation of its cementite lamellae, or thinly stacked layers (**Figure 4A**). However, after 30 minutes, the lamellae begin spheroidizing into small spheres along the grain boundaries (**Figure 4B**). This observation further suggests that induction heating accelerates microstructural evolution, especially since pearlite spheroidization typically occurs only after exceptionally long hold times.

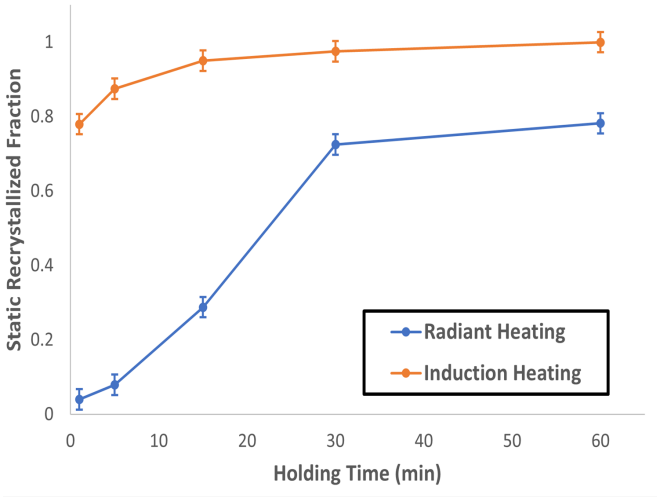

Figure 5: Static recrystallization fraction as a function of holding time for both heating methods. The recrystallized fraction was calculated using Equation 1 with normalized hardness values collected from each heating profile (holding time) for both radiant (blue) and induction heating (orange). Error bars represent the standard deviation, and two-tailed t-tests were used to determine statistical significance between both heating methods (p = 0.005).

In an effort to quantify the visual differences between the induction-heated and radiant-heated samples, we calculated the statically recrystallized (SRX) fraction, or the extent that a material has been fully recrystallized, as a function of hold time from hardness measurements (**Figure 5**). For the same heat treatment profile, the SRX fraction is greater for samples subject to induction heating compared to radiant heating. Specifically, this is seen with the induction-heated samples reaching an SRX fraction of 0.78 ± 0.3 after one minute, while the radiant-heated samples only reached the same SRX fraction after 60 minutes (**Figure 5**).

To further examine the effects of induction heating on SRX kinetics, we analyzed OM images using ImageJ software to measure grain size and grain density via the planimetric method. The characteristics of SRX grains obtained after induction heating and radiant heating are compared in the two microstructures having the closest recrystallized fraction, respectively, after a 60-minute hold time in the muffle furnace and after a one-minute hold time in the induction heater (**Figures 3B, 3G**). Despite having SRX fractions that are approximately equal, the induction-heated sample has a higher SRX grain density and a smaller grain size as calculated through average grain area (**Table 1, Figures 3B, 3G**). This suggests that induction heating greatly accelerates the nucleation of SRX grains.

OM images also reveal crucial differences between the edge and center microstructures in both the induction-heated and radiantly-heated samples (**Figures 6A-D**). For both

https://doi.org/10.59720/24-273

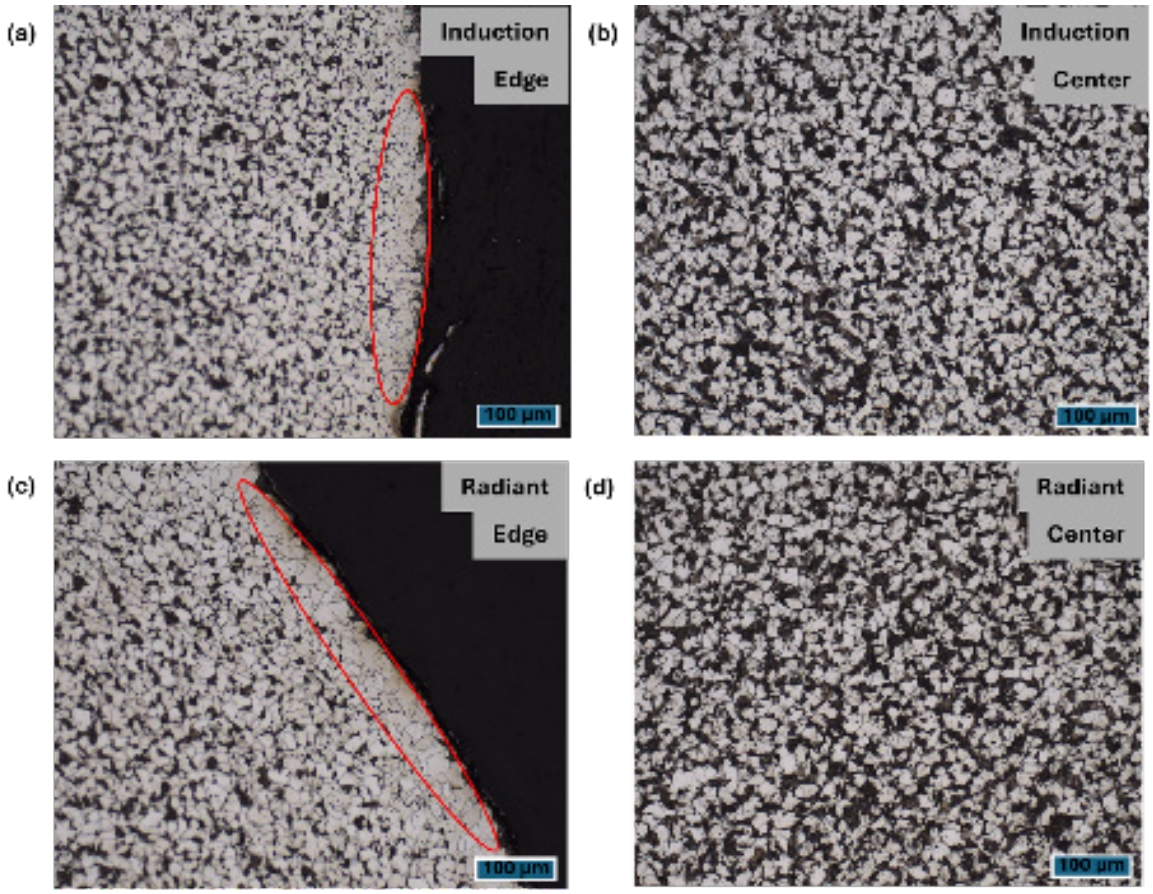

Figure 6: Unexpected microstructural differences observed at the edges and centers of samples for both heating methods. A comparison of etched OM images is shown for a sample inductively heated for (A, B) 5 minutes and radiantly heated for (C, D) 15 minutes. Within the samples, the light gray regions are ferrite, and the darker regions are pearlite. Increases in ferrite phase fraction (p = 0.001) and layer depth (p = 0.0015) are qualitatively observed at the edges of each sample (A, C) as denoted by red ovals and shown to be statistically significant with two-tailed t-tests. Notably, this effect is more significant in the inductively heated samples than in the radiant-heated samples.

heating methods, OM images from the sample edge show an increased ferrite phase composition compared to the center (**Figures 6A, 6C**). An analysis of OM images of the induction-heated samples using ImageJ software yielded an average ferrite phase composition of 83.6 ± 1.8% at the edge, whereas the center yielded 51.5 ± 1.9%. The radiantly-heated samples show a similar narrative, with an average ferrite phase composition of 86.4 ± 2.5% at the edge compared to 53.2 ± 3.1% at the center. Additionally, despite having a hold time of 10 minutes less, the layer in which this phenomenon of increased ferrite occurs is noticeably larger in the induction-heated samples (**Figures 6A, 6C**). ImageJ analysis reveals that the layer for the induction-heated samples is 92.1 ± 4.3 µm wide compared to only 63.3 ± 3.7 µm in the radiantly-heated samples. This difference may be attributed to the skin effect in induction heating.

DISCUSSION

Overall, our results confirm the hypothesis that induction heating accelerates SRX kinetics in AISI 4130 steel compared to radiant heating. Induction-heated samples demonstrated an earlier onset and faster rate of SRX, with more new, nucleating grains resulting in higher grain density and smaller grain size. Additionally, induction heating produced notable microstructural differences, including a thicker ferrite layer at the sample edge and early signs of pearlite spheroidization.

The significantly larger grain density and smaller grain size in induction-heated samples, despite a higher SRX fraction, provide insight into the accelerated nucleation process (**Table 1, Figure 5**). Literature commonly agrees that as new grains nucleate as a result of RX, they compete and collide with each other, forming grain boundaries (4, 7-10, 12). Thus, the large grain density and crowded nature of microstructures strongly support the conclusion that accelerated nucleation of grains occurs in induction-heated materials. Additionally, the consistent, faster softening of the induction-heated samples compared to the radiant-heated ones further illustrates the increased RX in induction heating (**Figure 2**). RX introduces new, smaller grains that relieve internal strain, reducing hardness and improving ductility. Decreased dislocation activation energy, possibly arising from electron-defect interactions enhancing atomic mobility, may explain this behavior. However, alternative factors such as rapid heating or localized gradients could also influence this behavior, necessitating further studies to verify this (**Figures 3B, 3D, 3F, 3H**).

Moreover, we observed early signs of pearlite spheroidization in induction-heated samples with hold

https://doi.org/10.59720/24-273

	Radiant Heat Treatment	Induction Heat Treatment
Respective OM Image	Figure 3G	Figure 3B
Hold Time (min)	60	1
Grain Area (μm²)	466	338
Grain Density (Grains/mm²)	2.2×10^3	3.0×10^3

Table 1: Comparing grain size and grain density for radiantly and inductively heated samples with similar SRX fractions. The planimetric method was used to determine grain size and grain density from the analyzed OM images.

times of 30 and 60 minutes (**Figures 3F, 3H, 4**). Pearlite spheroidization typically occurs after extremely long exposure to high temperatures, usually around 72 to 100 hours of holding below the lower critical temperature (22). For AISI 4130 steel, the lower critical temperature is approximately 723 °C. Thus, the presence of rapid pearlite spheroidization at such short hold times strongly suggests accelerated microstructure evolution in AISI 4130 steel when heated via induction heating. To our knowledge, this is the fastest pearlite spheroidization observed in AISI 4130 steel using a traditional heating profile. However, it is important to note that rapid pearlite spheroidization can also occur in other heating profiles, such as cyclic heat treatment, where samples are repeatedly heated and quenched in succession (22).

Furthermore, we observed differences in microstructure evolution at the edges and centers of samples subjected to both heat treatment methods (**Figures 6A-D**). Because the ferrite phase has a significantly lower carbon concentration than the pearlite microstructure, the decrease in the overall carbon content along the edges due to decarburization explains the higher number of ferrite grains present there. However, this decarburization layer was noticeably larger in the induction-heated samples despite a shorter hold time, suggesting that both skin effect and decarburization occurred simultaneously (**Figures 6A, 6C**). The skin effect refers to the tendency of alternating current to concentrate near the surface of a conductor, leading to localized surface heating and grain changes. We cannot deconvolve the two effects due to the similarity in thickness and microstructure evolution of the skin effect layer and the decarburization layer, so this cannot be confirmed. Nevertheless, the larger ferrite grain size development near the edge of the sample still provides evidence supporting the implications of the skin effect (**Figure 6A**). This likely results from the higher temperature gradient allowing the edge of the sample to enter the RX growth stage earlier than other portions of the sample. However, without further study, whether this phenomenon results from decarburization, the skin effect, or both remains unclear.

As such, substantial evidence supports accelerated SRX and microstructure evolution in AISI 4130 steel when heated via induction heating. Prior literature reports increased RX rate caused by electric current-based heating systems, and our results extrend these findings to include induction heating technologies and AISI 4130 steel (7-10). However, the exact physical mechanisms behind this interaction and how SRX kinetics are impacted are still not fully understood. The literature generally assumes that interactions between electrons and crystal defects cause the influence that electric current flow has on microstructural evolution (4). Since the movement of these crystal defects, such as dislocations, generally participate in SRX, the proposed interactions between electrons and crystal defects can be considered a possible cause of this phenomenon. It is also interesting to note the unexpected pearlite spheroidization we observed in this study. We propose that this rapid spheroidization can also be a direct result of electron-crystal defect interactions induced through induction heating and high driving forces for RX caused by high strain rates. However, this phenomenon is beyond the scope of this investigation and requires further study to confirm. Nevertheless, it is important to note that pearlite spheroidization generally enhances machinability and ductility, making it particularly advantageous for cold forming processes in the automotive industry (2).

Despite significant data supporting the accelerated SRX kinetics and microstructure evolution of AISI 4130 steel samples heated through induction heating, some limitations in this study may have skewed the results. Firstly, samples may not have all received the same strain during the initial deformation phase. Although we compressed samples as uniformly as possible, we sectioned them in half to avoid the dead metal zone since the highest concentration of strain exists in the center of a compressed material. This half-sectioning may not have achieved fully accuracy, potentially leading to differences in their respective strains. Secondly, due to limited time, we only made a single batch of samples per heat treatment profile, limiting the amount of data that could be collected. However, we collected data from each sample thoroughly across multiple measurements and imaging of multiple parts of the sample surface to ensure accuracy.

Although we thoroughly explored the effects of induction heating on microstructure evolution and SRX kinetics of AISI 4130 steel, there is still room for future research. As previously mentioned, the interactions between electrons and crystal defects, such as dislocations, remain unknown. Further work must investigate the skin effect and pearlite spheroidization in induction-heated AISI 4130 steel samples to develop optimized heating pathway profiles. Nevertheless, this work begins to address some of the fundamental gaps hindering the expansion of induction heating into more industrial applications and thus provides an efficient alternative to traditional radiant heating methods.

MATERIALS AND METHODS

Material Preparation

The material used for this study was AISI 4130 steel, which is generally considered to be a low to medium-carbon steel alloy. AISI 4130 steel, with a mill-specified composition (wt%) of 0.28C-0.46Mn-0.21Si-0.90Cr-0.21Mo, was received as a

https://doi.org/10.59720/24-273

cold-finished steel bar in the ferrite/pearlite microstructure. Samples were then heat-treated in a muffle furnace at 900ºC for 60 minutes, followed by 650ºC for 20 minutes, to homogenize the microstructure and remove any possible residual stress. Using an Allied Techcut 4x™ low-speed saw, cylindrical specimens with a diameter of 9.5 mm and a height of 5 mm were sectioned into four equal pie-shaped pieces to reduce the surface area to a point such that the yield stress required for compression is within the capabilities of the compression machine.

The samples were then deformed under compression with a fixed reduction in height of approximately 40%. This value was selected based on previous literature that constructed the Johnson-Mehl-Avrami-Kolmogorov (JMAK) equation for AISI 4130 steel and subsequent stress-strain curves (12). Initial deformation of the AISI 4130 steel samples was performed using an INSTRON® Compression Testing Machine with a maximum compressive force of 50 kN. Molybdenum disulfide (MoS_2) was used as a lubricant to coat all surfaces, reducing friction and preventing barreling of the samples. After compression, residual MoS_2 was gently removed by brushing the sample surfaces, with all handling performed using gloves to prevent contamination.

Radiative and Inductive Heat Treatment Procedures

This study focused specifically on the RX phenomena occurring at one working temperature, 700ºC, which was selected based on previous literature involving the RX of AISI 4130 steel (12). Experimental tests for RX were conducted under the same heat treatment profiles using two different heating methods: radiant and induction.

For the radiant heat treatments, the AISI 4130 steel samples were placed in the center of the Thermolyne™ Muffle Furnace. Temperature readings were held constant and measured by a Type K thermocouple positioned in the back of the furnace.

For the induction heat treatments, the AISI 4130 steel samples were placed directly in the center of the working zone. An induction solenoid coil with a fixed working frequency of around 280 kHz was positioned vertically around the samples. Since the samples could not be firmly clamped to the working zone, heating rates had to be slowed down to allow the samples to adapt to changes in the magnetic field and flux. A blackbody radiation Yokogawa pyrometer was used to measure the sample surface temperature with high precision at temperatures above 224ºC. The center of the working zone was marked by a red laser from the pyrometer, which was kept constant throughout all experiments and was located at the center of the sample surface.

Following compression, the cold-deformed samples were annealed at the target temperature of 700ºC for hold times of 1, 5, 15, 30, and 60 minutes (**Figure 1**). Samples were placed in their respective heating system at room temperature and then heated up to the target temperature. As measured in preliminary trials, the heating rate for the muffle furnace was around 0.53ºC/s, while the heating rate for the induction heater was kept at approximately 1.08ºC/s. The hold times began upon reaching the target temperature. Afterward, the samples were immediately water quenched after being removed from the muffle furnace or induction heater.

Microstructure Analysis

Grinding, polishing, and etching techniques were used to reveal the microstructure of the AISI 4130 steel samples. Specifically, samples were progressively ground using silicon-carbide sandpaper with grits ranging from 240 to 1200. Then, the samples were polished using six and one µm diamond suspension on microfiber polishing clothes. Finally, the polished sample surfaces were etched using a 2% Nital solution applied via the swab technique for 20 seconds. Afterward, samples were immediately rinsed with water to prevent further etching and remove any residual contaminants.

Microhardness measurements were collected using a Vickers microhardness indenter with an applied load of 0.3 kg. These measurements were taken from each sample five times in different spots near the center of the sample surface. By normalizing the hardness values, the SRX fraction was calculated using **Equation 1**, where H is the recrystallized hardness, HM is the maximum hardness, Hm is the minimum

$$X = 1 - (H - H_M)/(H_M - H_m) \qquad (1)$$

hardness, and X is the statically recrystallized fraction (12):

The SRX fraction describes the change in hardness resulting from the softening of a material that generally occurs due to SRX. In other words, it indicates the degree of SRX at each investigated condition.

Microstructural observations were gathered with a ZEISS Axiovert 5 optical microscope (OM) and a scanning electron microscope (SEM). Grain size measurements and phase fraction analysis were systematically conducted with 20x and 50x magnification OM images using ImageJ, an image processing software. Specifically, the planimetric method was used for grain size measurements, which calculates grain density by manually counting grains in known areas while excluding intersecting boundary grains to avoid bias. Phase fractions of ferrite and pearlite were determined through color thresholding of the acquired OM images. Observations of pearlite spheroidization were made using high-resolution SEM images taken at a magnification of 10,000x.

Statistical Analysis

Two-tailed t-tests were conducted to compare induction and radiant heating conditions using raw and processed data, including means, standard deviations, and sample sizes, to assess statistical significance. All relevant data, including recrystallized fraction, microhardness values, phase fraction, and skin effect layer, were reported with the mean, standard deviation, and p-value. A significance threshold of a p-value less than 0.01 ($p < 0.01$) was utilized throughout this study, and all four relevant data sets were well within this threshold.

ACKNOWLEDGMENTS

We would like to thank the University of Florida Center for Pre-Collegiate Education and Training (UF CPET) and the Student Science Training Program (SSTP) for supporting this work. We would also like to acknowledge the Nanoscale Research Facility (NRF) of the Herbert Wertheim College of Engineering at the University of Florida, where this work was partly conducted. Funding for this project was provided by the Forging Industry Educational and Research Foundation (FIERF).

https://doi.org/10.59720/24-273

Received: August 27, 2024
Accepted: July 22, 2025
Published: April 30, 2026

REFERENCES

1. "Automotive Motor Market Size & Share Report, 2019-2025." www.grandviewresearch.com/industry-analysis/automotive-motor-market. Accessed 13 Aug 2024.
2. Callister, William D. *Materials Science and Engineering: An Introduction*. John Wiley & Sons, 2007.
3. Humphreys, F. J. and Hatherly, M. *Recrystallization and Related Annealing Phenomena*. Elsevier, 2004.
4. Nicolaÿ, A., et al. "Influence of Joule Effect Heating on Recrystallization Phenomena in Inconel 718." *Metallurgical and Materials Transactions A*, vol. 52, no. 10, Oct. 2021, pp. 4572–96, https://doi.org/10.1007/s11661-021-06411-5.
5. Xu, Qing, et al. "Accumulation and Annihilation Effects of Electropulsing on Dynamic Recrystallization in Magnesium Alloy." *Materials Science and Engineering: A*, vol. 528, no. 7–8, Mar. 2011, pp. 3249–52, https://doi.org/10.1016/J.MSEA.2010.12.101.
6. Rudnev, Valery, et al. *Handbook of Induction Heating. 2nd ed.* CRC Press, Taylor & Francis Group, 2017.
7. Conrad, Hans. "Effects of Electric Current on Solid State Phase Transformations in Metals." *Materials Science and Engineering: A*, vol. 287, no. 2, Aug. 2000, pp. 227–37, https://doi.org/10.1016/S0921-5093(00)00780-2.
8. Xu, Zhen Sheng, et al. "Effect of Electric Current on the Recrystallization Behavior of Cold Worked α - Ti." *Scripta Metallurgica*, vol. 22, no. 2, Jan. 1988, pp. 187–90, https://doi.org/10.1016/S0036-9748(88)80331-4.
9. Krawczynska, Agnieszka T., et al. "Recrystallization and Grain Growth in Nano-structured Austenitic Stainless Steel under Electric Current Heating." *Physica Status Solidi c*, vol. 7, no. 5, May 2010, pp. 1380–83, https://doi.org/10.1002/pssc.200983377.
10. Huang, Ke, et al. "The Surprising Influence of Continuous Alternating Electric Current on Recrystallization Behaviour of a Cold-Rolled Aluminium Alloy." *Materials Characterization*, vol. 129, July 2017, pp. 121–26, https://doi.org/10.1016/J.MATCHAR.2017.04.036.
11. Walker, J., et al. "What Is the Best Method for Preheating 4130?" *Welding Journal*, vol. 93, no. 1, Jan. 2014, https://www.arcspecialties.com/wp-content/uploads/2019/08/AWS-Induction-Heating-1-1-3.pdf.
12. Tavakoli, Mohammad, et al. "Static Recrystallization Kinetics of Ferrite in Cold-Deformed Medium Carbon Steel." *Materials Research Express*, vol. 6, no. 12, 2019, https://doi.org/10.1088/2053-1591/ab6895.
13. Galligan, J. M. "Dislocation Drag Mechanisms in Normal State Metals." *Scripta Metallurgica*, vol. 18, no. 7, July 1984, pp. 653–56, https://doi.org/10.1016/0036-9748(84)90314-4.
14. Xi, Guoqiang, et al. "Effects of Induction Quenching on the Recrystallization Behavior of a Twin-Structured Mg-Mn Alloy." *Journal of Materials Engineering and Performance*, vol. 33, no. 7, Apr. 2024, pp. 3353–73, https://doi.org/10.1007/s11665-023-08212-w.
15. Ambrogio, Giuseppina, et al. "Induction Heating and Cryogenic Cooling in Single Point Incremental Forming of Ti-6Al-4V: Process Setup and Evolution of Microstructure and Mechanical Properties." *International Journal of Advanced Manufacturing Technology*, vol. 91, no. 1–4, July 2017, pp. 803–12, https://doi.org/10.1007/s00170-016-9794-7.
16. Lu, Zhen, et al. "Evolution of Grain Boundary Character Distribution in Near-Surface Regions of a Cold-Rolled Nickel-Based Superalloy during Induction Heating Process." *Journal of Materials Research and Technology*, vol. 15, Nov. 2021, pp. 801–09, https://doi.org/10.1016/J.JMRT.2021.08.086.
17. Conrad, Hans, et al. "Effect of Prior Cold Work on the Influence of Electric Current Pulses on the Recrystallization of Copper." *Scripta Metallurgica*, vol. 18, no. 3, Mar. 1984, pp. 275–80, https://doi.org/10.1016/0036-9748(84)90522-2.
18. Bao, W., et al. "Electro-Plastic Effect on Tensile Deformation Behaviour and Microstructural Mechanism of AZ31B Alloy." *Materials Science and Technology*, vol. 33, no. 7, May 2017, pp. 836–45, https://doi.org/10.1080/02670836.2016.1242272.
19. Cryderman, Robert, et al. "Effects of Rapid Induction Heating on Transformations in 0.6% C Steels." *Journal of Materials Engineering and Performance*, vol. 29, no. 6, Feb. 2020, pp. 3502–15, https://doi.org/10.1007/s11665-020-04632-0.
20. Topolski, Łukasz, et al. "Methods for Determining Power Losses in Cable Lines with Non-Linear Load." *Przeglad Elektrotechniczny*, vol. 94, no. 9, 2018, pp. 85–90, https://doi.org/10.15199/48.2018.09.21.
21. Smith, William F. *Structure and Properties of Engineering Alloys*. McGraw-Hill, 1993.
22. Maity, Joydeep, et al. "Mechanism of Accelerated Spheroidization of Steel during Cyclic Heat Treatment around the Upper Critical Temperature." *Philosophical Magazine Letters*, vol. 93, no. 4, Apr. 2013, pp. 231–37, https://doi.org/10.1080/09500839.2012.758390.